NeuroImage: Clinical 24 (2019) 102023

Contents lists available at ScienceDirect

NeuroImage: Clinical

journal homepage: www.elsevier.com/locate/ynicl

Resting-state functional connectivity predicts individual language impairment of patients with left hemispheric gliomas involving language network

Binke Yuan[a,1], Nan Zhang[b,c,1], Jing Yan[d,1], Jingliang Cheng[d], Junfeng Lu[c], Jinsong Wu[c,e,*]

[a] Center for Language and Brain, Shenzhen Institute of Neuroscience, Shenzhen, China
[b] Department of Neurosurgery, The First Affiliated Hospital of USTC, Division of Life Sciences and Medicine, University of Science and Technology of China, Hefei, Anhui, China
[c] Glioma Surgery Division, Department of Neurosurgery, Huashan Hospital, Fudan University, Shanghai, China
[d] Department of MRI, The First Affiliated Hospital of Zhengzhou University, Zhengzhou, China
[e] Shanghai Key Laboratory of Medical Image Computing and Computer Assisted Intervention, Shanghai, China

ARTICLE INFO

Keywords:
Low-grade glioma
High-grade glioma
Resting-state fMRI
Language
Machine learning

ABSTRACT

Language deficits following brain tumors should consider the dynamic interactions between different tumor growth kinetics and functional network reorganization. We measured the resting-state functional connectivity of 126 patients with left cerebral gliomas involving language network areas, including 77 patients with low-grade gliomas (LGG) and 49 patients with high-grade gliomas (HGG). Functional network mapping for language was performed by construction of a multivariate machine learning-based prediction model of individual aphasia quotient (AQ), a summary score that indicates overall severity of language impairment. We found that the AQ scores for HGG patients were significantly lower than those of LGG patients. The prediction accuracy of HGG patients (R^2 = 0.27, permutation P = 0.007) was much higher than that of LGG patients (R^2 = 0.09, permutation P = 0.032). The rsFC regions predictive of LGG's AQ involved the bilateral frontal, temporal, and parietal lobes, subcortical regions, and bilateral cerebro-cerebellar connections, mainly in regions belonging to the canonical language network. The functional network of language processing for HGG patients showed strong dependence on connections of the left cerebro-cerebellar connections, limbic system, and the temporal, occipital, and prefrontal lobes. Together, our findings suggested that individual language processing of glioma patients links large-scale, bilateral, cortico-subcortical, and cerebro-cerebellar functional networks with different network reorganizational mechanisms underlying the different levels of language impairments in LGG and HGG patients.

1. Introduction

A brain tumor is a mass or growth of abnormal cells in the brain. Gliomas are the most common primary brain tumors. Diffusive and progressive glioma infiltration of healthy tissues leads to significant functional reshaping and behavioral or cognitive deficits (e.g., language impairment or aphasia). Most previous structural or functional MRI (fMRI) studies (Huang et al., 2018; Lu et al., 2017; Weng et al., 2018; Zhang et al., 2016), as well as intraoperative electrocortical stimulation studies (Duffau et al., 2014; Picart et al., 2018; Sanai et al., 2008; Wu et al., 2015), attempted to localize the surrounding eloquent functional areas to maximize the extent of tumor resection while reducing the risk of postoperative cognitive deficits. The patterns of functional and structural alterations following glioma growth have been explored, including the recruitment of perilesional regions as local reorganization, homotopic reorganization of gray matter volume (Almairac et al., 2018), activation changes in the contralesional homologous region (Chivukula et al., 2018; Desmurget et al., 2007), and the remote recruitment of other ipsihemispheric and contrahemispheric regions, such as the cerebellum (Zhang et al., 2018). These local

Abbreviations: LGG, low-grade glioma; HGG, high-grade glioma; ABC, Aphasia Battery of Chinese; AQ, aphasia quotient; SS, spontaneous speech

* Corresponding author at: Glioma Surgery Division, Neurosurgery Department of Huashan Hospital, Shanghai Medical College, Fudan University, Shanghai 200040, China.
E-mail address: wjsongc@126.com (J. Wu).

[1] These authors contributed equally to this work.

https://doi.org/10.1016/j.nicl.2019.102023
Received 12 June 2019; Received in revised form 5 September 2019; Accepted 27 September 2019
Available online 19 October 2019

and remote adaptive mechanisms have been thought to be physiological basis for the high level of functional reorganization and are used to explain why tumor infiltration within the so-called “eloquent” areas often does not result in detectable neurological deficits. However, relatively few studies have focused on language network reorganization of the brain following glioma growth.

In contrast to the long-lasting localizationist view of language neurobiology as residing solely in Broca's and Wernicke's areas, numerous pieces of convincing evidences indicated that language function relies on interconnected cortico-subcortical regions and bilaterally-distributed connections, forming the language network (Duffau et al., 2014; Fedorenko and Thompson-Schill, 2014; Luo et al., 2019; Torres-Prioris et al., 2019; Tremblay and Dick, 2016). In this delocalized network-based framework, language regions in the frontal, temporal and parietal lobes, and the right cerebellum are structurally and/or functionally connected, forming large-scale language (sub) networks for linguistic processing.

Due to the infiltrative, diffusive, and migratory characteristics of gliomas, pathological perturbations by tumor are rarely confined to a single locus but instead influence other regions via axonal pathways (Fornito et al., 2015; Hillary and Grafman, 2017; Stam, 2014). Numerous reports have shown that brain tumors can lead to various cognitive deficits-related alterations in local and interhemispheric resting-state functional connectivity (rsFC) across different functional networks (Fox and King, 2018; Ghinda et al., 2018). We have shown that left hemispheric gliomas induce language-related structural and functional alterations in cerebellum via cerebro-cerebellar circuits (Zhang et al., 2018). Outside the language network, diffused functional reorganization may occur in the contralesional hemisphere and other functional systems (Fox and King, 2018; Ghinda et al., 2018), allowing both long-distance and global lesion effects. Brain tumors also cause significant alterations in global network topology, such as global network efficiency (Aerts et al., 2016).

Notably, the severity of cognitive deficits, network disruptions, and the degree of network reorganization are related to the speed of infiltration and the extent to which the tumor infiltrates healthy functional systems (Aerts et al., 2016; Fox and King, 2018; Ghinda et al., 2018; Zhang et al., 2018). Tumor grade is an important predictor of patients’ clinical and cognitive deficits (Taphoorn and Klein, 2004). In the World Health Organization (WHO) grading system, grade I tumors are the least malignant and grade III or IV tumors are the most malignant. Grade I and II brain tumors are often referred to as low-grade gliomas (LGG), whereas grade III and IV are described as high-grade gliomas (HGG). Previous studies have shown that LGG patients with slow infiltration (infiltration over a time period of years) typically have extensive functional reshaping and only slightly impaired or undetectable language deficits (Duffau, 2005; Zhang et al., 2018). In contrast, HGG patients (infiltration over a time period of months) exhibit more severe language and other cognitive impairments than LGG patients (Desmurget et al., 2007; Noll et al., 2015; van Kessel et al., 2017; Zhang et al., 2018). Additionally, several studies reported that LGG and HGG patients had different plastic mechanisms of brain networks (van Dellen et al., 2012; Zhang et al., 2016). However, no study has attempted to investigate the language network basis at the whole brain level to determine the language network reorganization differences between LGG and HGG patients.

In this work, a large sample of 126 patients, including 77 patients with LGGs and 49 patients with HGGs, were subjected to machine learning-based network mapping for language. All patients included in this study have left cerebral gliomas involving language network areas. For each patient, we measured rsFC using a whole-brain parcel (Shen et al., 2013) after excluding the patient's tumor extent. For each group, we then built a machine leaning-based rsFC prediction model of individual language scores. The language-related network for each model was identified based on predictive contribution (i.e., the highest predictive weights). We hypothesized that glioma would induce widespread network disruptions, including the language network. The perilesional intact language regions, the ipsilesional and contralesional (homologous) language regions, and the cerebellum and cerebro-cerebellar circuits may participate in language processing. The reliability of the findings was evaluated by further considering different preprocessing/analysis strategies (i.e., the parcellation scheme, covariates, global signal removal, feature selection threshold and generalizability of the prediction model).

2. Materials and methods

2.1. Participants

Patients were prospectively screened and collected from two centers: 1) Huashan Hospital (from 2011 to 2016), and 2) the First Affiliated Hospital of Zhengzhou University (from 2014 to 2018). Because we used the same system of MRI scanner (Siemens Magnetom Verio 3.0 T MRI), as well as identical imaging protocols and inclusion criteria, the data from the two centers were analyzed together and a potential site effect was controlled by adding the site factor as a single regressor in the statistical analysis.

Patient inclusion criteria: (1) Pathologically confirmed glioma (based on 2007 WHO classification system) in left cerebral hemisphere (Louis et al., 2007); (2) No chemo and/or radiation treatment history; (3) Location of the glioma overlapped or was within the language network areas proposed by Fedorenko et al. (2010); (4) Patients’ age was 18–75 years old; (5) Right-handedness confirmed by the Edinburgh Handedness Inventory; (6) No symptoms of motor impairment, as indicated by a score of grade V on the Medical Research Council (MRC) Scale for Muscle Strength (Paternostro-Sluga et al., 2008); (7) Chinese Han nationality; (8) No history of brain surgery; (9) More than nine years of education; (10) No midline shift in structural images, as confirmed by the *in situ* location of midline structures (corpus callosum, septa pellucidum, third ventricle, hypothalamus, and pineal region) of the brain; (11) Both structural and functional images covered the whole brain, especially the whole cerebellum; (12) Good cooperation during the linguistic/cognitive evaluation; (13) No history of other major neurological or psychiatric disorders; and (14) No history of alcohol or drug abuse.

In total, 126 patients met all inclusion criteria and completed the entire preoperative clinical, language, and imaging data acquisition. The patients were further grouped based on the malignancy of brain tumors: 77 patients with grade I (n = 2) and II (n = 75) brain tumors were designated as low-grade gliomas (LGG) and 49 patients with grade III (n = 26) and IV (n = 23) brain tumors were designated as high-grade gliomas (HGG). For the two cases of grade I in LGG group, one patient was diagnosed as ganglio glioma and the other patient was diagnosed as neuroepithelial glioma.

All patients underwent comprehensive assessment of Karnofsky performance status, language, motor, and general cognitive function (Zhang et al., 2018). The language function was assessed using the Aphasia Battery for Chinese speakers (ABC). ABC is the Chinese standardized adaptation of the Western Aphasia Battery (Lu et al., 2013; Wu et al., 2015; Zhang et al., 2018), and includes spontaneous speech (range, 0–20), comprehension (range, 0–230), repetition (range, 0–100), and naming (range, 0–100) scores. The Aphasia Quotient (AQ) score (range, 0–100) can be calculated from these items to reflect the global severity. The demographics and clinical information are summarized in Table 1. The language scores from the ABC tests for the two groups are presented in Supplementary Fig. 1.

All processes strictly followed the requirements of the Declaration of Helsinki. This study was approved and supervised by the Ethics Committee of Huashan Hospital and the Ethics Committee of the First Affiliated Hospital of Zhengzhou University, respectively. Written informed consents were obtained from all subjects and/or their legal guardians.

Table 1
Demographic information and language scores of LGG and HGG patients

	LGG (n = 77)	HGG (n = 49)	χ^2 or t	P value
Age	38.84 ± 9.65	43.27 ± 14.71	−2.04	0.04
Gender (M/F)	44/33	29/20	0.22[a]	0.82[a]
Education	10.92 ± 4.07	11.35 ± 4.28	−0.56	0.58
Tumor volume (cm^3)	82.34 ± 49.99	77.22 ± 49.58	0.56	0.57
FD	0.07 ± 0.03	0.08 ± 0.04	−1.2	0.25
WHO grade	I/II = 2/75	III/IV = 26/23	-	-
AQ	95.23 ± 4.84	91.75 ± 8.11	3.02	0.003
Spontaneous speech	18.86 ± 1.48	18.12 ± 2.39	2.13	0.035
Comprehension	222.27 ± 13.09	213.92 ± 22.55	2.63	0.009
Repetition	96.82 ± 6.64	94.51 ± 10.11	1.56	0.12
Naming	94.06 ± 5.64	88.05 ± 10.83	4.09	0.001

WHO, World Health Organization; AQ, Aphasia Quotient; FD, framewise displacement.
[a] P-value obtained using Pearson's chi-square test.

2.2. Image acquisition

For LGG, high resolution T1-weighted and T2-weighted fluid-attenuated inversion recovery (T2-FLAIR) images were acquired with the following parameters. T1-weighted images: axial magnetization-prepared rapid gradient echo (MPRAGE) sequence, repetition time (TR) = 1900 ms; echo time (TE) = 2.93 ms; flip angle (FA) = 9°; inversion time (TI) = 900 ms; field of view (FOV) = 250 × 219 mm; matrix size = 256 × 215; slice thickness = 1 mm; voxel size = 1 × 1 × 1 mm^3; slice number = 176; and scanning time = 7 min 47 s. T2-FLAIR: TR = 9000 ms; TE = 99 ms; FA = 150°; TI = 2500 ms; FOV = 240 × 214 mm; matrix size = 256 × 160; slice thickness = 2 mm; voxel size = 0.9 × 1.3 × 2.0 mm^3; slice number = 66; and scanning time = 7 min 30 s. For HGG, the T1-weighted sequence images with contrast (gadopentetate dimeglumine) were acquired with the same parameters.

For all patients, rs-fMRI images were acquired using the following parameters: TR = 2000 ms; TE = 35 ms; FA = 90°; FOV = 240 × 240 mm^2; matrix size = 64 × 64; thickness/gap = 4 mm/1 mm; voxel size = 3.3 × 3.3 × 5.0 mm^3; slice number = 33; scanning time = 8 min; and number of time points = 240. All subjects were required to remain still with their eyes closed and not fall asleep during the time of scanning.

2.3. Structural data processing

Lesion mapping. For each patient, manual tumor drawing on the 3D-T1 images was performed based on the contrast-enhancing tumor areas or the FLAIR hyperintense areas (necrotic areas were included but not peritumoral edema). For 3D-T1 images without glioma enhancement, T2-FLAIR images were first coregistered to the 3D-T1 images to serve as visual reference. After manually tracing the tumor, we created a 3D-T1 volume lacking the tumor area (set to 0) for each patient. This procedure was performed manually using RANO criteria as reference (Wen et al., 2010). The accuracy of the manual tracing was then confirmed by a senior neurosurgeon. Each 3D-T1 volume without tumor area was segmented into gray matter (GM), white matter (WM), cerebrospinal fluid (CSF), bone, soft tissue, and air/background using SPM12 (https://www.fil.ion.ucl.ac.uk/spm). The cost function masking method was used to improve the precision of spatial normalization in glioma patients (Andersen et al., 2010). We then used DARTEL (Diffeomorphic Anatomical Registration using Exponentiated Lie algebra) for registration, normalization, and modulation (Ashburner, 2007). A customized template was generated using the average tissue probability maps across all subjects, and then each subject's segmented maps were

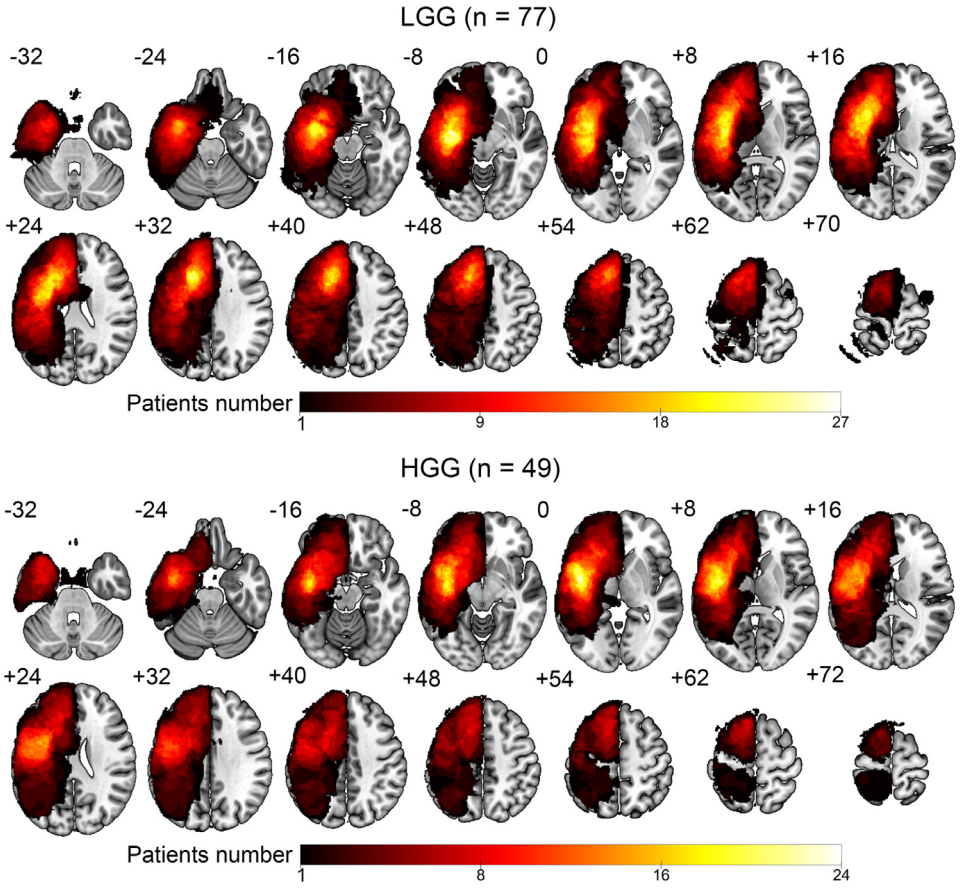

Fig. 1. Lesion topography of the 77 LGG patients and 49 HGG patients. The color bar represents the number of patients with a lesion on a specific voxel.

warped into the template. This procedure was repeated until the best study-specific template was generated. The images were then modulated according to the Jacobian determinants to ensure conservation of regional differences in the absolute amounts of GM. Finally, the registered images were transformed to Montreal Neurological Institute (MNI) space. The native tumor mask was spatially normalized to standard MNI space by applying the deformation field estimated by segmentation. Tumor masks of each group (LGG or HGG) in MNI space were then stacked and binarized to construct a tumor-overlapping image (Fig. 1), in which each voxel was identified as part of the tumor region from at least one patient.

2.4. Functional data processing

Only fMRI signals in intact voxels were considered in the following analyses. The first 10 volumes were discarded, and then slice timing and motion correction were performed. No patients exhibited a head motion >3 mm maximum translation or 3° rotation. The motion-corrected functional images were first co-registered to the 3D-T1 images and were then spatially normalized into the MNI space by applying the deformation field estimated in segmentation. The normalized images were spatially smoothed using a Gaussian kernel (Full width at half maximum of 6 mm). The linear trend and the nuisance signals (36 parameters, including the *x, y, z* translations and rotations) + WM/CSF/global time courses (9 parameters), plus their temporal derivatives (9 parameters) and the quadratic terms of 18 parameters (Ciric et al., 2017; Satterthwaite et al., 2013) were removed by linear regression from each voxel's time course. Then, temporal band-pass filtering (0.01–0.1 Hz) was performed on the residuals. A 'scrubbing' procedure was additionally adopted to reduce any head motion artifact (Power et al., 2012; Yan et al., 2013). Specifically, rs-fMRI volumes that showed sudden head motion, based on the criterion of framewise displacement (FD) above 0.5 mm (Power et al., 2012, 2015, 2014) were discarded, together with one volume before and two volumes after the bad volume. No patient had volumes less than 140. Voxel-wise temporal signal-to-noise ratio (tSNR) was estimated after spatial normalization (Molloy et al., 2014; Triantafyllou et al., 2005), and was averaged over voxels in a whole brain mask. The whole brain mask was the binarized image of a brain parcellation atlas (Shen et al., 2013) used for network construction and feature extraction (described in the next section). Patients were excluded if the whole brain mean tSNR was less than 40.

2.5. Functional connectivity

Whole brain resting-state functional connectivity (rsFC). We adopted a functional brain parcellation atlas including 268 nodes (Shen et al., 2013) for network construction because this parcellation scheme included subcortical regions and cerebellum and was developed based on rsFC homogeneity. Individual functional networks were constructed by calculating the Pearson's correlation coefficients between pairwise nodes (268 × 268). The *r* values in each matrix were transformed to *z* values using Fisher's *r*-to-*z* transformation. If a node fully injured, its connections with other nodes were set to 0.

Structural and functional data preprocessing was performed using SPM (http://www.fil.ion.ucl.ac.uk/spm) and Data Processing Assistant for Resting-State fMRI software (DPARSF; Chao-Gan and Yu-Feng, 2010; Yan et al., 2016; available at http://rfmri.org/DPARSF). The network construction was performed using the Graph-theoretical Network Analysis Toolkit (GRETNA; Wang et al., 2010; available at http://www.nitrc.org/projects/gretna/).

2.6. Machine learning-based brain-language prediction model

A schematic overview of our prediction framework is presented in Fig. 2. A rsFC feature selection procedure (Dosenbach et al., 2010) was

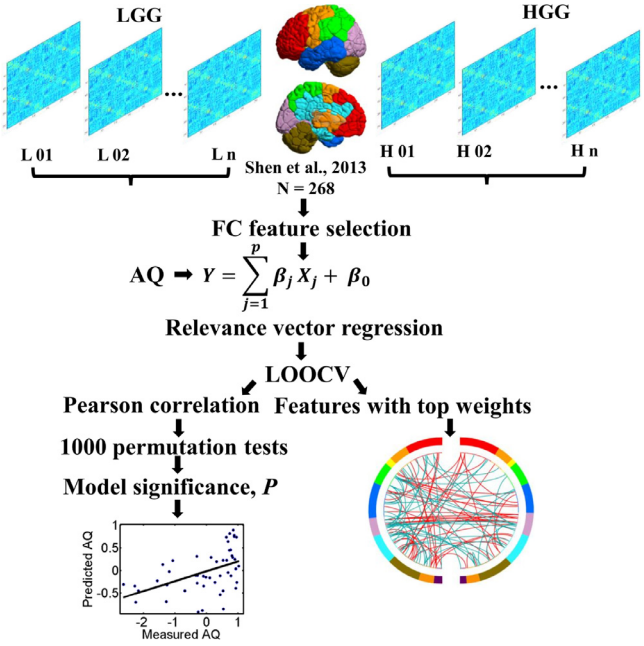

Fig. 2. Schematic overview of the analysis framework. For each patient, a patient-specific whole brain atlas excluding the tumor volume was created and then used to construct a whole-brain resting-state functional connectivity (rsFC) matrix. The lower triangle elements of the matrix were extracted as the initial whole-brain rsFC feature vector. The rsFC whole brain features were used to predict the Aphasia Quotient (AQ) scores of LGG or HGG patients by relevance vector regression (RVR). In each model, a nested leave-one-out-cross-validation (LOOCV) was applied and the prediction accuracy was evaluated by calculating the Pearson correlation coefficient between the predicted labels and real labels. The model significance was calculated based on 1000 permutation tests. For models with significant prediction (permutation $P < 0.05$), features with top weights were extracted.

implemented by ranking features according to their degrees of correlation coefficients with the AQ values, retaining only features with the highest correlation coefficients corresponding to a P value < .005. The initial univariate feature-filtering step has been shown to improve overall model performance (Martino et al., 2008; Pereira et al., 2009). Note that we chose AQ as dependent variable because it reflected the global severity of language impairment.

Linear relevance vector regression (RVR). We selected to use RVR due to its demonstrated high prediction performance in brain-behavior/cognition mapping (Cui and Gong, 2018). RVR is a Bayesian framework for learning sparse regression models. It does not include an algorithm-specific parameter, so does not require extra computational resources for parameter estimation (Tipping, 2000). In RVR, only some samples (fewer than the training sample size), termed the 'relevance vectors', are used to fit the model:

$$y(x) = \sum_{i=1}^{m} w_i \tau_i + \in \quad (1)$$

where $\tau_i$are basis functions, and $\in$is normally distributed with mean 0 and variance β. RVR uses the training data to build a regression model:

$$y = \theta\omega + \in \quad (2)$$

where $y = [y_1, y_2, \ldots y_n]^T$, $\theta = [\theta_1, \theta_2, \ldots \theta_n]$, $\theta_i = [\tau_i(x_1), \tau_i(x_2), \ldots \tau_i(x_n)]^T$. Each vector θ_i consists of the values of basis function τ_i for the input vectors and is a relevance vector.

The model parameters βwere determined by using the maximum likelihood estimates from the conditional distribution: $p(y \mid \alpha, \beta) = \mathcal{N}(y \mid 0, C)$, where $C = \beta I_n + \Phi A^{-1}\Phi^T$. To generate the RVM favor sparse regression models, prior distributions were assumed for both $w_i$and β^{-1}, i.e., $p(w_i \mid \alpha_i) = \mathcal{N}(0, \alpha_i^{-1})$ and resulted in the

same relevance vector machine construction. After finding the optimal point estimates for parameters α_i and β, the point estimate w for weight vector w was obtained from the equation $w = \beta(\beta\Phi^T\Phi + A)^{-1}\Phi^T y$.

Prediction accuracy and significance. Leave-one-out-cross-validation (LOOCV) was used to calculate the prediction accuracy (the Pearson correlation coefficient between the predicted and actual labels). For each round of LOOCV, one patient was designated as the test sample and the remaining patients were used to train the model. The predicted score was then obtained from the feature matrix of the tested sample.

The significance level was computed based on 1000 permutation tests. For each permutation test, the prediction labels (i.e., the patients' AQ) were randomized, and the same RVR prediction process used for the actual data was carried out. After 1000 permutations, a random distribution of accuracies was obtained and the P value was correspondingly calculated as: $P = \frac{number\ of\ permutaion\ tests < actural\ accuracy + 1}{number\ of\ permutaion\ tests + 1}$.

Exploration of the weight-based language network. The feature weight indicates the importance of each feature in the regression model. For the significant prediction models (permutation $P < 0.05$), the most predictive connections with the highest absolute weights were extracted. For each rsFC-based prediction model of AQ, the top 100 rsFC connections were extracted. In the linear RVR model, connections with positive weights indicate that increased rsFC predicts better performance, and connections with negative weights indicate that increased rsFC predicts worse performance.

For illustration purpose, we summed the absolute weights for each node of all its top connections, so the size of each node is relative to its total contribution to the model. rsFCs with top weights were then classified into six different types to determine the network lateralization: interhemispheric positive, interhemispheric negative, left or right intrahemispheric positive, and left or right intrahemispheric negative (Siegel et al., 2016). Finally, the numbers of rsFCs belonging to each of the six types were counted for each model.

2.7. Validation analysis

We validated our main results (model significance and top predictors) by further considering the following variables: 1) *Parcellation scheme.* To determine if our major results were affected by the specific brain parcellation scheme used, we repeated the prediction analyses using another brain parcellation—the Brainnetome atlas (Fan et al., 2016). The Brainnetome Atlas ($n = 246$) was defined using both anatomical landmarks and connectivity-driven information. The anatomical regions defined by Desikan et al. (2006) were parcellated into subregions based on functional and structural connectivity data from 40 adults. Because the Brainnetome atlas only includes cortical and subcortical parcels, we created a whole brain parcellation ($n = 271$) by adding the well-established cerebellum subregions ($n = 25$) created by Buckner et al. (2011) to the Brainnetome Atlas. 2) *Covariates*. we found that age was statistically significantly correlated with language scores for both LGG and HGG patients (Supplementary Table 1). Education showed statistically significant correlations with the language scores of HGG patients. We also found weak correlations of individual mean FD (Power et al., 2012; Yan et al., 2013) and tumor volume with language scores for both LGG and HGG patients. To minimize potential confounding effects of these covariates in model prediction, we calculated the partial correlations between the predicted AQ scores and the observed AQ scores including sex, age, education, FD, tumor volume, and site as covariates. 3) *Global signal removal.* Global signal removal is a controversial preprocessing step and recent work suggested that different preprocessing strategies may provide complementary insights into functional brain organization (Murphy and Fox, 2017). Global signal removal was performed in the main analysis to suppress the motion effect (Power et al., 2015), and we also reanalyzed our data without regressing out the global signal. 4) *Feature selection threshold*. We examined the effects of different feature selection significance thresholds on our main results by comparing the results with different feature selection thresholds (i.e., P value $< .05$ and P value $< .01$). 5) *Generalizability*. To assess the generalizability of the prediction model, we applied 10-fold cross-validation (Cui and Gong, 2018). For each group (i.e., LGG and HGG), all patients were divided into 10 subsets. To prevent random bias between subsets, we sorted the subjects according to their AQ scores and then assigned individuals with a rank of (1st, 11th, 21th, …) to the first subset, (2nd, 12th, 22th, …) to the second subset, …, and (10th, 20th, 30th, …) to the tenth subset. Of the 10 subsets, 9 were combined as the training set, and the remaining subset was used as the testing set. A prediction model was constructed using all the training samples and then used to predict the scores of the testing samples. The Pearson correlation coefficients between the actual scores and the predicted scores were computed to quantify the accuracy of the prediction. The training and testing procedures were repeated 10 times so that each of the 10 subsets was used once as the testing set. To yield the final accuracies, we averaged the correlations across the 10 iteration. The significance level was computed based on 1000 permutation tests.

3. Results

3.1. Demographics and language deficits in LGG and HGG patients

There was no significant difference in gender, education, FD, and tumor volumes between LGG and HGG patients (Table 1). Patients in the HGG group were of significantly higher age than those in the LGG group (two sample t-test, $t(124) = 2.144$, $P = 0.037$). More than 20% (17/77) of LGG patients had AQ scores less than 93.8, a clinical criterion of an aphasic subject. More than 45% (22/49) patients had AQ scores less than 93.8 (Supplementary Fig. 1). HGG patients had significantly lower AQ (two sample t-test, $t(124) = 3.02$, $P = 0.003$), spontaneous speech (two sample t-test, $t(124) = 2.13$, $P = 0.035$), comprehension (two sample t-test, $t(124) = 2.63$, $P = 0.009$), and naming scores (two sample t-test, $t(124) = 4.09$, $P = 0.001$) compared to the LGG patients. The repetition scores of HGG patients were lower than those of LGG patients, but did not have statistical significance (two sample t-test, $t(124) = 1.56$, $P = 0.12$).

To see whether the language differences between LGG and HGG groups were due to the age difference or site effect, we then performed two-sample t-test for each kind of language test by adding age, sex, education, tumor volume, and site as covariates. After controlling for these potential confounding factors, we found that AQ ($t(119) = 2.81$, $P = 0.006$), comprehension ($t(119) = 2.75$, $P = 0.007$), and naming ($t(119) = 3.87$, $P = 1.7\text{E}-4$) scores of HGG patients were significantly lower than those of LGG patients. The spontaneous speech ($t(119) = 1.61$, $P = 0.11$) and repetition scores ($t(119) = 1.27$, $P = 0.208$) of HGG patients were lower than LGG patients but did not reach statistical significance.

3.2. Whole-brain rsFCs predict AQ scores for both LGG and HGG patients

As shown in Fig. 3, the generated rsFC-based RVR models significantly predicted AQ scores for both LGG ($r = 0.299$, permutation $P = 0.032$) and HGG patients ($r = 0.521$, permutation $P = 0.007$). For each model, the top 100 rsFC features that exhibited the highest predictive power were extracted and projected back onto the brain (Fig. 4).

For LGG patients, nodes with top weights were distributed in the bilateral inferior frontal gyrus (IFG), middle frontal gyrus (MFG), superior frontal gyrus (SFG), anterior temporal lobe (ATL), middle temporal gyrus (MTG), inferior temporal gyrus (ITG), the inferior parietal lobe (IPL), the dorsal anterior cingulate cortex (dACC), fusiform, insula, subcortical regions, the posterior cerebellum, the brainstem, and the right middle occipital gyrus (MOG).

For HGG patients, the nodes with top weights were distributed in the bilateral IFG, MFG, SFG, ATL, MTG, STG, ITG, insula, subcortical

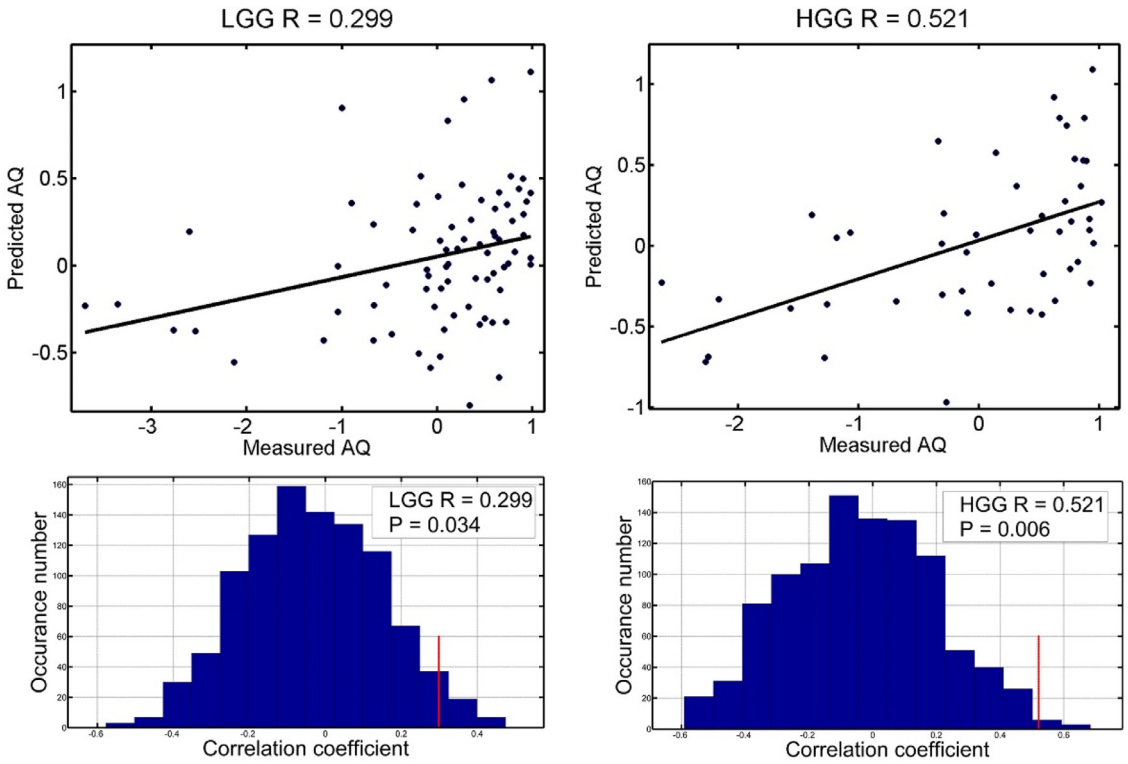

Fig. 3. The rsFC-AQ model accuracies of the LGG and HGG groups. The scatter plots (normalized within each group) of actual and predicted AQ scores and the corresponding linear fitted lines are shown. The *R* values are the Pearson correlation coefficients between the predicted values and the actual values. The histograms indicate model significance with calculated *P* values based on 1000 permutation tests.

regions, MOG, calcarine, precentral and postcentral gyrus, middle cingulate gyrus, precuneus, fusiform, the posterior cerebellum, the right IPL, angular gyrus, cuneus, and the brainstem. The right medulla oblongata had the highest weight, with connections to the precentral gyrus, ATL, MFG, and subcortical regions.

The connections of each rsFC-AQ model were further divided into subgroups. As shown in Fig. 5A, there were fewer ipsilesional intrahemispheric connections (15 vs 25) and more interhemispheric connections (55 vs 46) in LGG model than HGG model, and a comparable number of contralesional intrahemispheric connections (30 vs 29) for the two models. When considering the weight sign (positive or negative, Fig. 5B): LGG vs HGG: interhemispheric positive, 0.29 vs 0.27; interhemispheric negative, 0.26 vs 0.19; L intrahemispheric positive: 0.06 vs 0.15; L intrahemispheric negative: 0.09 vs 0.1; R intrahemispheric positive: 0.12 vs 0.15; R intrahemispheric negative: 0.18 vs 0.14).

We then assessed the predictive contribution of each anatomical network by averaging the weights of all nodes belonging to each network. As shown in Fig. 5D, the temporal, prefrontal, cerebellum, limbic, and parietal networks showed the most predictive contributions for the LGG model, and the cerebellum, limbic, temporal, occipital, and prefrontal networks showed the most predictive contributions for the HGG model.

For both LGG and HGG models, nodes with top weights in the cerebellum included the bilateral cerebellar lobule VI, Crus I, Crus II, and VIIa. The regions with the highest weights in the right cerebellar lobule were Crus I and Crus II for LGG models and the regions with the highest weights in the left cerebellar lobule were IV-V, VI, VIII, X and the right pons for HGG patients (Figs. 4–6). Given the importance of the cerebro-cerebellar circuits in language processing, we calculated the number of connections from nodes in the cerebellum or brainstem to nodes in cortical and subcortical regions. For the 100 connections with top weights in each model, there were more cerebro-cerebellar connections present in the HGG model than in the LGG model, 37 vs 49 (Fig. 5C). The subtype numbers of cerebro-cerebellar connections in the LGG and HGG models were: ipsilesional intrahemispheric connections: 3 vs 19, interhemispheric connections: 19 vs 20, and contralesional intrahemispheric connections: 15 vs 11 (Fig. 6).

For LGG patients, the rsFC models of spontaneous speech ($r = 0.359$, permutation $P = 0.033$) and comprehension ($r = 0.299$, permutation $P = 0.034$) scores were significant.

3.3. Validation results

The validation results are summarized in Supplementary Tables 2 and 3.

The effect of Parcellation scheme. When using the Brainnetome atlas, rsFCs significantly predicted HGG patient's AQ ($r = 0.473$, permutation $P = 0.015$) and repetition ($r = 0.398$, permutation $P = 0.016$) scores. All models for LGG patients did not perform well.

The effect of Covariates. We found that controlling for potential confounding variables did not change the model significance and correlations between real scores and predicated scores were only slightly changed.

The effect of global signals. Without removal of global signals, there were significant predictive accuracies in the rsFC models for HGG patient's AQ ($r = 0.539$, permutation $P = 0.003$) and LGG patient's naming ($r = 0.344$, permutation $P = 0.02$) scores.

The effect of rsFC feature selection threshold. When using a *P* value of 0.05 for rsFC feature selection, the predictive accuracies were significant in the rsFC models of HGG patient's AQ ($r = 0.454$, $P = 0.004$), repetition ($r = 0.251$, $P = 0.049$) and naming ($r = 0.278$, $P = 0.04$) scores. A positive trend of significance was observed for LGG patient's AQ ($r = 0.21$, $P = 0.06$) scores.

When using a *P* value of 0.01 for rsFC feature selection, the predictive accuracies were significant in the rsFC models of LGG patient's AQ ($r = 0.372$, $P = 0.01$), comprehension ($r = 0.237$, $P = 0.049$) scores, and for HGG patient's AQ ($r = 0.478$, $P = 0.007$) scores.

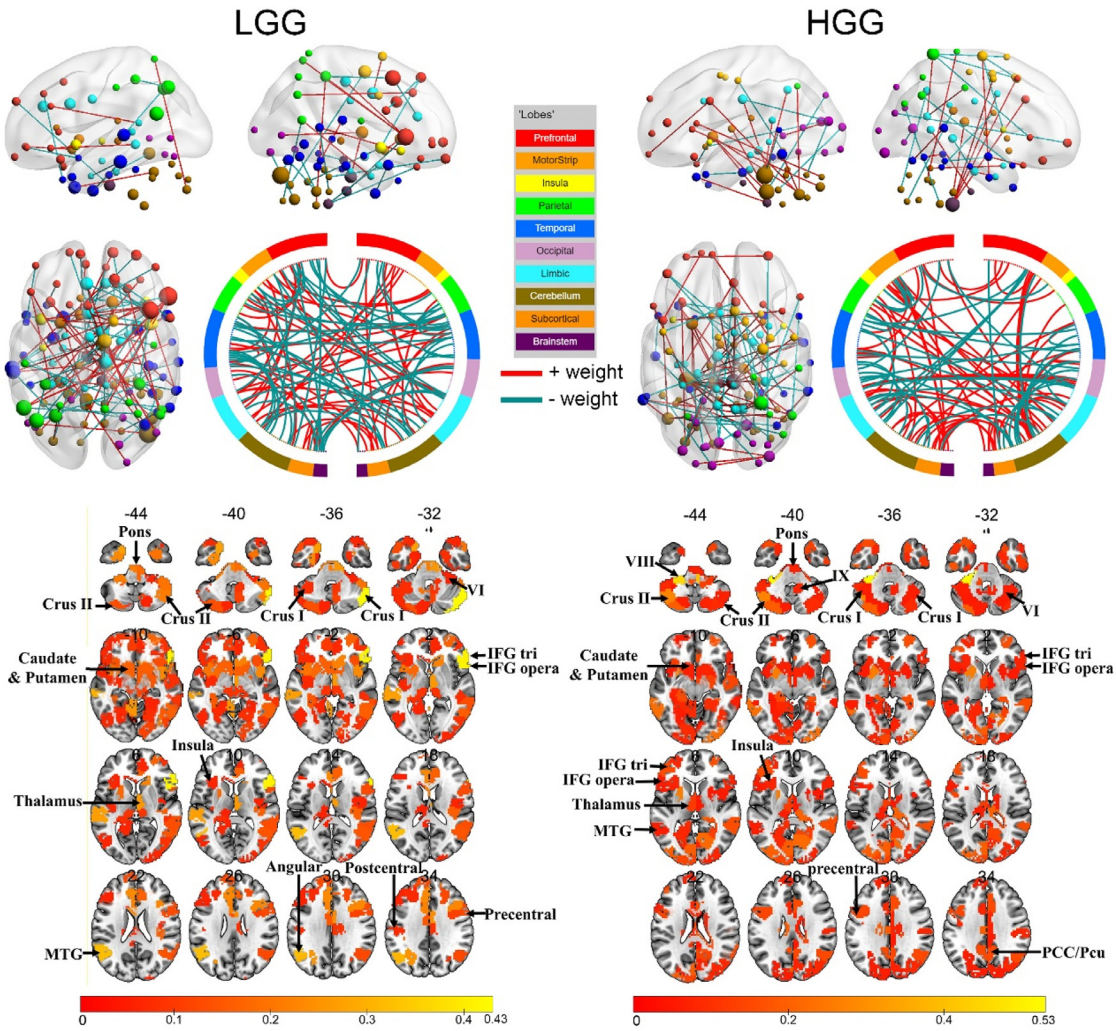

Fig. 4. The most predictive connections and regions for each rsFC-AQ model. Top: the 100 rsFCs with the highest absolute weights were projected back onto a brain surface or shown in the circle plot. Red connections indicate positive weights (increased rsFC predicts better performance), and green connections indicate negative weights (increased rsFC predicts worse performance). The subset of the 268 parcels (Shen et al., 2013) included in the top 100 connections are displayed as spheres. The node sizes are proportional to the total contribution of each node (the sum of the absolute weights of the node) to the model. Bottom: the subset of the 268 parcels included in the top 100 connections displayed in an axial view. The rsFCs and regions with top weights were mapped onto the cortical surfaces using the BrainNet Viewer package (Xia et al., 2013; available at http://www.nitrc.org/projects/bnv/).

10-folder cross-validation. We found that rsFC-based RVR models significantly predicted AQ scores for HGG patients ($r = 0.496$, permutation $P = 0.013$) and comprehension scores ($r = 0.493$, permutation $P = 0.002$) for LGG patients. Positive trends of significance were observed for LGG patient's AQ ($r = 0.288$, $P = 0.056$) and repetition ($r = 0.283$, $P = 0.058$) scores.

4. Discussion

In this study, we performed functional network mapping of language by predicting aphasia scores based on the connectome-based functional connectivity for patients with left cerebral glioma involving language network. The main findings were as follows: 1) HGG patients showed more severe language impairments than LGG patients; 2) The rsFC model of HGG patients accounted for > 27% of language variance, a percentage that was much higher than that of LGG patients (model only accounted for 0.09 of language variance); 3) For LGG patients, regions predictive of language impairments involved canonical language regions distributed in the left frontal, temporal, and parietal lobes, the subcortical regions, the right cerebellum and homotopic regions, whereas the language-related network of HGG patients showed heavy dependence on the left cerebellum, the right brainstem, the limbic system, and the temporal, prefrontal, and occipital lobes.

To our knowledge, this is the first study using a machine-learning prediction model to investigate the large-scale whole brain language network basis of patients with left cerebral glioma involving language network.

4.1. Individualized language prediction of glioma patients

We found that the language impairments of glioma patients could be significantly predicted by whole-brain functional connectivity, especially for HGG patients with severe language deficits. Our results are consistent with those of previous studies which found that language deficits after focal brain damage, especially tumors, traumatic brain injury, and stroke, could be predicted based on disruptions of network connectivity (Fang et al., 2015; Siegel et al., 2016; Warren et al., 2014; Yourganov et al., 2016). We also found much higher model accuracy of HGG patients than that of LGG patients. Numerous results have shown that slow infiltrative LGGs (generally over years) induce great plasticity within the central nervous system, often resulting in undetectable or only slight neurological deficits (Duffau, 2005; Zhang et al., 2018). This

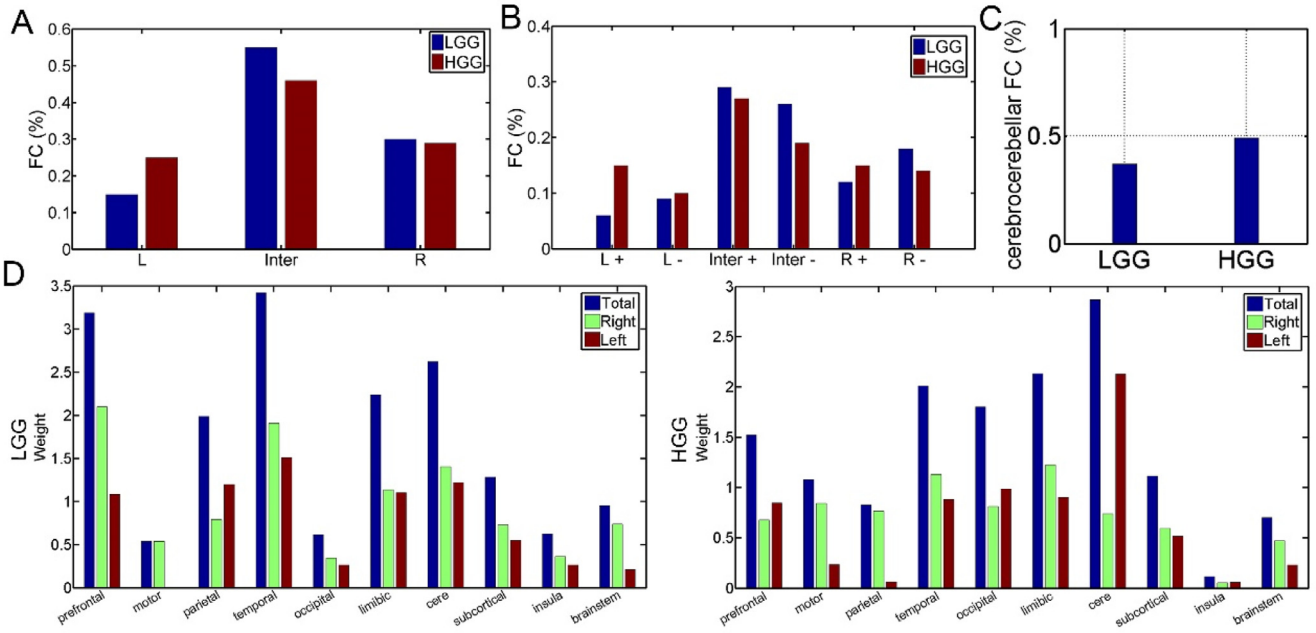

Fig. 5. The distributions of the 100 most predictive connections. A: Connections are divided into three groups: ipsilesional intrahemispheric (L), interhemispheric (Inter), and contralesional intrahemispheric (R). (B): Connections are further divided into six groups based on the sign of the connection weight (+: positive; -negative). (C): The percentages of the cerebrocerebellar connections in each model. (D): The relatively predictive contributions of each predefined network based on anatomy. For each network, the weights of all nodes belonging to this network were summed.

means that although there may be marked structural or functional changes in LGG patients (Almairac et al., 2018; Zhang et al., 2018), there was weak or no imaging-behavioral correlation. The strong brain-behavior relationship in HGG patients may be because the rapid (generally several months) and diffused growth of tumor cells infiltrating the normal brain tissue overwhelms the network plasticity and induces more severe and diverse language deficits as well as network disruptions.

4.2. Different network bases for language processing in LGG and HGG

In this work, we showed the functional connections of delocalized regions to support language processing for glioma patients. For both LGG and HGG, rsFC regions predictive of AQ involved canonical cerebral language areas, including the left IFG, STG, MTG, TP, the superior and posterior parietal cortex, insula, subcortical regions, and their homotopic regions. The recruitment of the right homotopic language regions has been well studied. In healthy (right-handed) subjects, right hemisphere language homologues, mainly the right IFG and the temporal lobe, participate in semantic, phonological, and syntactic processing (Tan et al., 2005; Vigneau et al., 2006; Kwok et al., 2019). For patients with left hemisphere damage, language-related structural and functional alterations have been frequently observed in the right hemisphere language homologues (Saur et al., 2008; Turkeltaub et al.,

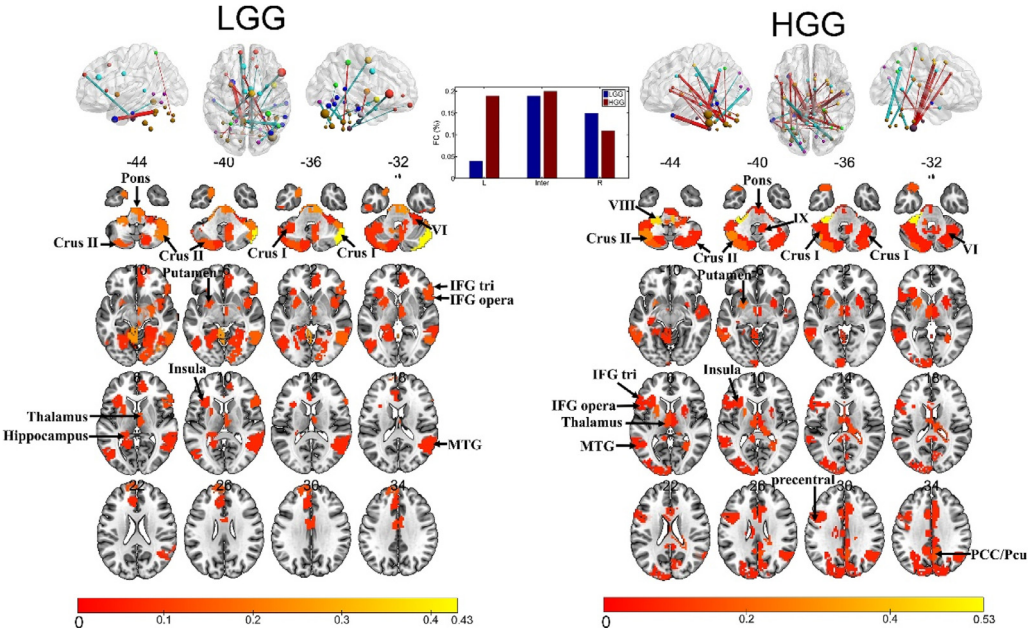

Fig. 6. The most predictive cerebro-cerebellar connections and regions for the two rsFC-AQ models.

2012; Winhuisen et al., 2007; Xing et al., 2016). However, the right hemisphere engagement may be maladaptive, i.e., the hyperactivity or hypertrophy of the right hemisphere is associated with poor language performance (Fornito et al., 2015; Hope et al., 2017). For patients with left language eloquent brain tumors, task-based functional MRI studies showed that preoperative LGG patients with tumors infiltrating classical Broca's, Wernicke's, or insula areas exhibited redistribution of compensatory activations in perilesional, remote ipsilesional, and contralesional homotopic language-related areas and slight dysphasia (Benzagmout et al., 2007; Duffau, 2012, 2005; Duffau et al., 2001; Robles et al., 2008; Sarubbo et al., 2012), suggesting a delocalized functional compensation. Brain stimulation studies showed that left language eloquent brain tumors changed the language dominance of the left hemisphere to the right hemisphere in a homotopic manner (Krieg et al., 2013; Thiel et al., 2005). In 15 patients with lesions involving the left-sided language-eloquent brain areas (MTG, STG, IFG, angular gyrus), Krieg and colleagues performed bilateral repetitive navigated transcranial magnetic stimulation language mapping by measuring the error rate of an object-naming task for left and right hemisphere stimulation. They found a functional language shift to the right hemisphere for both LGG and HGG patients exhibiting left-sided language function during awake brain surgery (Krieg et al., 2013). Additionally, suppressing or enhancing non-damaged right hemisphere language homotopic regions can improve language performance in patients with aphasia (Naeser et al., 2011; Turkeltaub et al., 2012).

There are obvious differences in the language network patterns of LGG and HGG patients. First, there are different predictive contributions of the canonical language regions for the two models. Temporal and prefrontal regions showed the most predictions in LGG models, but the connections in the cerebellum, limbic system, the temporal, occipital, and prefrontal lobes were leading predictors in the HGG model. Second, based on the distribution and predictive contribution of rsFC, the language network of LGG is right-lateralized, but no obvious lateralization was observed in HGG patients. These observations are consistent with the findings by Thiel et al. (2005) who showed that a tumor-grade related shift from the left to the right, i.e., LGG patients showed a higher degree of integration of the right hemisphere into the language network after left hemisphere glioma than HGG patients. Third, different cerebro-cerebellar circuits are implicated in language processing for LGG and HGG patients.

4.3. The cerebro-cerebellar circuits implicated in language processing for both LGG and HGG patients

The roles of the cerebellum and cerebro-cerebellar circuits in language processing have been verified in neuroanatomical, neuroimaging, and clinical studies (Buckner, 2013; De Smet et al., 2013; Mariën et al., 2017). Anatomically, the cerebro-cerebellar circuit consists of two loops in an approximately homotopic manner. The feedbackward (output) loop originates from the cerebellum and projects to the motor (motor and premotor cortex) and non-motor cerebral association areas (e.g., prefrontal cortex, the supplementary motor area, the superior temporal and posterior parietal regions, cingulate gyrus, the parahypocampal region and the limbic cortices) via the motor and non-motor nuclei of the thalamus. The feed-forward (input) loop originates from the cerebral cortex and sends projections or inputs to the contralateral cerebellar cortex via the ipsilateral pons (corticopontine and pontocerebellar mossy fiber pathways). Disruptions in specific cerebro-cerebellar circuits could contribute to different behavioral symptoms. The right cerebellum (i.e., the right cerebellar lobule VI, Crus I, Crus II) is mainly involved in language, with a topographic organization of the lateralized linguistic cerebellum (Marien et al., 2001). Cerebellar damage induces functional suppression to distal regions that are anatomically and functionally connected supratentorial regions due to the decrease or loss of transmission of excitatory impulses from the deep nuclei of the cerebellum via the cerebello-ponto-thalamo-cerebral pathways to the supratentorial brain regions, a phenomenon named cerebello-cerebral diaschisis.

Our previous work also showed the vital role of the cerebellum and cerebro-cerebellar circuits in language network reorganization for glioma patients following supratentorial lesion (Zhang et al., 2018). In LGG patients, the cerebellar areas with significantly decreased spontaneous activity exhibited significantly increased rsFC with high-order cognitive related supratentorial areas, including the right thalamus, ACC, and posterior cingulate cortex. We extended our previous findings and showed that a left supratentorial tumor lesion induced network reorganization of cerebro-cerebellar circuits for both LGG and HGG patients. In LGG patients, a right lateralized cerebro-cerebellar connectivity pattern was observed, with the right cerebellar lobule Crus I as the most predictive region, suggesting a nearly normal cerebro-cerebellar circuit for language processing. In HGG patients, more left hemispheric cerebro-cerebellar connections were identified, with the most predictive regions as the left cerebellar lobule IV-V, VI, VIII and X, and the right medulla oblongata. The shifting of the cerebro-cerebellar circuits to the ipsilesional side as observed in HGG patients suggested disruptions by the left supratentorial glioma of the functionally lateralized cerebro-cerebellar circuits for language and a homotopic cerebro-cerebellar circuits emerged to support language processing.

4.4. Non-language functional systems that support language processing

In addition to the language network, several non-language functional systems were also found, such as the limbic system for both LGG and HGG models and the occipital and motor networks for HGG models. The implication of them may be because the language network showed high interactions with the functional systems involved in visual processing, motor processing, emotion processing, executive control, working memory, and default model network (Duffau et al., 2014; Hernández et al., 2019; Siegel et al., 2016; Xu et al., 2016). Language deficits can be induced by the disruptions of bilaterally distributed support processes, such as visual attention required for reading or motor planning for speech (Connor et al., 2000; Otten et al., 2012), and language recovery is highly related to the recovery of memory and attention (Ramsey et al., 2017).

5. Limitations

There are several limitations of this study.

First, prediction accuracy and stability of machine learning models are both exponentially related to the sample size, where a minimum sample size of 200 is needed to achieve highest model performance (Cui and Gong, 2018). Although we adopted data from two centers, the two study groups were small (LGG: 77 patients; HGG: 49 patients). A large sample size from other centers will be needed to reach stable and higher model performance and also ensure the representativeness of the results (Corbetta et al., 2015).

Second, the overall prediction accuracies of the two groups, especially the LGG group, are relatively low (r values, 0.2–0.5). Focal tumor damage can induce both structural and functional changes and joint prediction with cooperating multi-modal imaging features (e.g., GM volume and white-matter connectivity) can improve prediction accuracy (Dai et al., 2012; Liem et al., 2017). However, considering the slight language impairments in most LGG patients, multi-modal features may not improve overall model accuracy due to the weak brain-behavior relationship.

Third, most of our patients were enrolled before 2016 and thus the pathological stratification in this study was based on the 2007 WHO classification system. Future studies that utilize the new 2016 WHO classification system are needed to delineate the language network reorganization for each molecular glioma subtype.

6. Conclusions

The whole-brain rsFCs prediction model can significantly predict the language variance of preoperative patients with left cerebral glioma, especially for HGG patients with more severe language impairments. For both LGG and HGG patients, large-scale language connections were identified which bilaterally distributed in prefrontal, temporal, and parietal lobes, posterior cerebellar lobule, limbic system, brainstem, and subcortical regions. Our results suggest a significant role of right hemisphere language homologues for LGG and a strong dependence of ipsilesional cerebro-cerebellar circuits for HGG. These results advance our understanding of the large-scale language network reorganization of preoperative glioma patients, and provide insight into why areas thought to be critical in language processing can be resected without inducing permanent deficit.

Funding

This work was supported by the Shenzhen Double Chain Grant [2018]256, China Postdoctoral Science Foundation (no. 2018M640825), Research Projects of Henan Higher Education (no. 18A320077), and The Scientific and Technological Research Projects of Henan Province (no. 192102310123).

CRediT authorship contribution statement

Binke Yuan: Data curation, Writing - original draft. **Nan Zhang:** Data curation, Writing - original draft. **Jing Yan:** Writing - original draft. **Jingliang Cheng:** Conceptualization, Supervision, Writing - original draft. **Junfeng Lu:** Conceptualization, Supervision, Data curation, Writing - original draft. **Jinsong Wu:** Conceptualization, Supervision, Data curation, Writing - original draft.

Declaration of Competing Interest

The authors declare no competing financial interests.

Acknowledgments

We gratefully acknowledge all patients that participated in the trial.

Supplementary materials

Supplementary material associated with this article can be found, in the online version, at doi:10.1016/j.nicl.2019.102023.

References

Aerts, H., Fias, W., Caeyenberghs, K., Marinazzo, D., 2016. Brain networks under attack: robustness properties and the impact of lesions. Brain 139, 3063–3083. https://doi.org/10.1093/brain/aww194.

Almairac, F., Duffau, H., Herbet, G., 2018. Contralesional macrostructural plasticity of the insular cortex in patients with glioma: a VBM study. Neurology 91, e1902–e1908. https://doi.org/10.1212/WNL.0000000000006517.

Andersen, S.M., Rapcsak, S.Z., Beeson, P.M., 2010. Cost function masking during normalization of brains with focal lesions: still a necessity? Neuroimage 53, 78–84. https://doi.org/10.1016/j.neuroimage.2010.06.003.

Ashburner, J., 2007. A fast diffeomorphic image registration algorithm. Neuroimage 38, 95–113. https://doi.org/10.1016/j.neuroimage.2007.07.007.

Benzagmout, M., Gatignol, P., Duffau, H., 2007. Resection of World Health Organization Grade II gliomas involving Broca's area: methodological and functional considerations. Neurosurgery 61, 741–743. https://doi.org/10.1227/01.NEU.0000298902.69473.77.

Buckner, R.L., 2013. The cerebellum and cognitive function: 25 years of insight from anatomy and neuroimaging. Neuron 80, 807–815. https://doi.org/10.1016/j.neuron.2013.10.044.

Buckner, R.L., Krienen, F.M., Castellanos, A., Diaz, J.C., Yeo, B.T., 2011. The organization of the human cerebellum estimated by intrinsic functional connectivity. J. Neurophysiol. 106, 2322–2345. https://doi.org/10.1152/jn.00339.2011.

Chao-Gan, Y., Yu-Feng, Z., 2010. DPARSF: A MATLAB toolbox for "pipeline" data analysis of resting-state fMRI. Front. Syst. Neurosci. 4, 13. https://doi.org/10.3389/fnsys.2010.00013.

Chivukula, S., Pikul, B.K., Black, K.L., Pouratian, N., Bookheimer, S.Y., 2018. Contralateral functional reorganization of the speech supplementary motor area following neurosurgical tumor resection. Brain Lang. 183, 41–46. https://doi.org/10.1016/j.bandl.2018.05.006.

Ciric, R., Wolf, D.H., Power, J.D., Roalf, D.R., Baum, G.L., Ruparel, K., Shinohara, R.T., Elliott, M.A., Eickhoff, S.B., Davatzikos, C., Gur, R.C., Gur, R.E., Bassett, D.S., Satterthwaite, T.D., 2017. Benchmarking of participant-level confound regression strategies for the control of motion artifact in studies of functional connectivity. Neuroimage 154, 174–187. https://doi.org/10.1016/j.neuroimage.2017.03.020.

Connor, L.T., Albert, M.L., Helm-Estabrooks, N., Obler, L.K., 2000. Attentional modulation of language performance. Brain Lang. 71, 52–55. https://doi.org/10.1006/brln.1999.2210.

Corbetta, M., Ramsey, L., Callejas, A., Baldassarre, A., Hacker, C.D., Siegel, J.S., Astafiev, S.V, Rengachary, J., Zinn, K., Lang, C.E., Connor, L.T., Fucetola, R., Strube, M., Carter, A.R., Shulman, G.L., 2015. Common behavioral clusters and subcortical anatomy in stroke. Neuron 85, 927–941. https://doi.org/10.1016/j.neuron.2015.02.027.

Cui, Z., Gong, G., 2018. The effect of machine learning regression algorithms and sample size on individualized behavioral prediction with functional connectivity features. Neuroimage 178, 622–637. https://doi.org/10.1016/j.neuroimage.2018.06.001.

Dai, Z., Yan, C., Wang, Z., Wang, J., Xia, M., Li, K., He, Y., 2012. Discriminative analysis of early Alzheimer's disease using multi-modal imaging and multi-level characterization with multi-classifier (M3). Neuroimage 59, 2187–2195.

De Smet, H.J., Paquier, P., Verhoeven, J., Marien, P., 2013. The cerebellum: its role in language and related cognitive and affective functions. Brain Lang. 127, 334–342. https://doi.org/10.1016/j.bandl.2012.11.001.

Desikan, R.S., Segonne, F., Fischl, B., Quinn, B.T., Dickerson, B.C., Blacker, D., Buckner, R.L., Dale, A.M., Maguire, R.P., Hyman, B.T., Albert, M.S., Killiany, R.J., 2006. An automated labeling system for subdividing the human cerebral cortex on MRI scans into gyral based regions of interest. Neuroimage 31, 968–980. https://doi.org/10.1016/j.neuroimage.2006.01.021.

Desmurget, M., Bonnetblanc, F., Duffau, H., 2007. Contrasting acute and slow-growing lesions: a new door to brain plasticity. Brain 130, 898–914. https://doi.org/10.1093/brain/awl300.

Dosenbach, N.U., Nardos, B., Cohen, A.L., Fair, D.A., Power, J.D., Church, J.A., Nelson, S.M., Wig, G.S., Vogel, A.C., Lessov-Schlaggar, C.N., Barnes, K.A., Dubis, J.W., Feczko, E., Coalson, R.S., Pruett Jr., J.R., Barch, D.M., Petersen, S.E., Schlaggar, B.L., 2010. Prediction of individual brain maturity using fMRI. Science 329, 1358–1361. https://doi.org/10.1126/science.1194144.

Duffau, H., 2012. The "frontal syndrome" revisited: lessons from electrostimulation mapping studies. Cortex 48, 120–131. https://doi.org/10.1016/j.cortex.2011.04.029.

Duffau, H., 2005. Lessons from brain mapping in surgery for low-grade glioma: insights into associations between tumour and brain plasticity. Lancet Neurol. 4, 476–486. https://doi.org/10.1016/S1474-4422(05)70140-X.

Duffau, H., Bauchet, L., Lehericy, S., Capelle, L., 2001. Functional compensation of the left dominant insula for language. Neuroreport 12, 2159–2163.

Duffau, H., Moritz-Gasser, S., Mandonnet, E., 2014. A re-examination of neural basis of language processing: proposal of a dynamic hodotopical model from data provided by brain stimulation mapping during picture naming. Brain Lang. 131, 1–10. https://doi.org/10.1016/j.bandl.2013.05.011.

Fan, L., Li, H., Zhuo, J., Zhang, Y., Wang, J., Chen, L., Yang, Z., Chu, C., Xie, S., Laird, A.R., Fox, P.T., Eickhoff, S.B., Yu, C., Jiang, T., 2016. The human brainnetome atlas: a new brain Atlas based on connectional architecture. Cereb. Cortex 26, 3508–3526. https://doi.org/10.1093/cercor/bhw157.

Fang, Y., Han, Z., Zhong, S., Gong, G., Song, L., Liu, F., Huang, R., Du, X., Sun, R., Wang, Q., He, Y., Bi, Y., 2015. The semantic anatomical network: evidence from healthy and brain-damaged patient populations. Hum. Brain Mapp. 36, 3499–3515. https://doi.org/10.1002/hbm.22858.

Fedorenko, E., Hsieh, P.J., Nieto-Castanon, A., Whitfield-Gabrieli, S., Kanwisher, N., 2010. New method for fMRI investigations of language: defining ROIs functionally in individual subjects. J. Neurophysiol. 104, 1177–1194. https://doi.org/10.1152/jn.00032.2010.

Fedorenko, E., Thompson-Schill, S.L., 2014. Reworking the language network. Trends Cogn. Sci. 18, 120–126. https://doi.org/10.1016/j.tics.2013.12.006.

Fornito, A., Zalesky, A., Breakspear, M., 2015. The connectomics of brain disorders. Nat. Rev. Neurosci. 16, 159–172. https://doi.org/10.1038/nrn3901.

Fox, M.E., King, T.Z., 2018. Functional connectivity in adult brain tumor patients: a systematic review. Brain Connect. 8, 381–397. https://doi.org/10.1089/brain.2018.0623.

Ghinda, D.C., Wu, J.S., Duncan, N.W., Northoff, G., 2018. How much is enough-can resting state fMRI provide a demarcation for neurosurgical resection in glioma? Neurosci. Biobehav. Rev. 84, 245–261. https://doi.org/10.1016/j.neubiorev.2017.11.019.

Hernández, M., Ventura-Campos, N., Costa, A., Miró-Padilla, A., Ávila, C., 2019. Brain networks involved in accented speech processing. Brain Lang. 194, 12–22. https://doi.org/10.1016/j.bandl.2019.03.003.

Hillary, F.G., Grafman, J.H., 2017. Injured brains and adaptive networks: the benefits and costs of hyperconnectivity. Trends Cogn. Sci. 21, 385–401. https://doi.org/10.1016/j.tics.2017.03.003.

Hope, T.M.H., Leff, A.P., Prejawa, S., Bruce, R., Haigh, Z., Lim, L., Ramsden, S., Oberhuber, M., Ludersdorfer, P., Crinion, J., Seghier, M.L., Price, C.J., 2017. Right hemisphere structural adaptation and changing language skills years after left hemisphere stroke. Brain 140, 1718–1728. https://doi.org/10.1093/brain/awx086.

Huang, H., Lu, J., Wu, J., Ding, Z., Chen, S., Duan, L., Cui, J., Chen, F., Kang, D., Qi, L.,

Qiu, W., Lee, S.W., Qiu, S., Shen, D., Zang, Y.F., Zhang, H., 2018. Tumor tissue detection using blood-oxygen-level-dependent functional MRI based on independent component analysis. Sci. Rep. 8, 1223. https://doi.org/10.1038/s41598-017-18453-0.

Krieg, S.M., Sollmann, N., Hauck, T., Ille, S., Foerschler, A., Meyer, B., Ringel, F., 2013. Functional language shift to the right hemisphere in patients with language-eloquent brain tumors. PLoS One 8, e75403. https://doi.org/10.1371/journal.pone.0075403.

Kwok, V.P.Y., Matthews, S., Yakpo, K., Tan, L.H., 2019. Neural correlates and functional connectivity of lexical tone processing in reading. Brain Lang. 196, 104662. https://doi.org/10.1016/j.bandl.2019.104662.

Liem, F., Varoquaux, G., Kynast, J., Beyer, F., Kharabian Masouleh, S., Huntenburg, J.M., Lampe, L., Rahim, M., Abraham, A., Craddock, R.C., Riedel-Heller, S., Luck, T., Loeffler, M., Schroeter, M.L., Witte, A.V., Villringer, A., Margulies, D.S., 2017. Predicting brain-age from multimodal imaging data captures cognitive impairment. Neuroimage 148, 179–188. https://doi.org/10.1016/j.neuroimage.2016.11.005.

Louis, D.N., Ohgaki, H., Wiestler, O.D., Cavenee, W.K., Burger, P.C., Jouvet, A., Scheithauer, B.W., Kleihues, P., 2007. The 2007 WHO classification of tumours of the central nervous system. Acta Neuropathol. 114, 97–109. https://doi.org/10.1007/s00401-007-0243-4.

Lu, J., Wu, J., Yao, C., Zhuang, D., Qiu, T., Hu, X., Zhang, J., Gong, X., Liang, W., Mao, Y., Zhou, L., 2013. Awake language mapping and 3-Tesla intraoperative MRI-guided volumetric resection for gliomas in language areas. J. Clin. Neurosci. 20, 1280–1287. https://doi.org/10.1016/j.jocn.2012.10.042.

Lu, J., Zhang, H., Hameed, N.U.F., Zhang, J., Yuan, S., Qiu, T., Shen, D., Wu, J., 2017. An automated method for identifying an independent component analysis-based language-related resting-state network in brain tumor subjects for surgical planning. Sci. Rep. 7, 13769. https://doi.org/10.1038/s41598-017-14248-5.

Luo, D., Kwok, V.P.Y., Liu, Q., Li, W., Yang, Y., Zhou, K., Xu, M., Gao, J.H., Tan, L.H., 2019. Microstructural plasticity in the bilingual brain. Brain Lang. 196, 104654. https://doi.org/10.1016/j.bandl.2019.104654.

Marien, P., Engelborghs, S., Fabbro, F., De Deyn, P.P., 2001. The lateralized linguistic cerebellum: a review and a new hypothesis. Brain Lang. 79, 580–600. https://doi.org/10.1006/brln.2001.2569.

Mariën, P., van Dun, K., Van Dormael, J., Vandenborre, D., Keulen, S., Manto, M., Verhoeven, J., Abutalebi, J., 2017. Cerebellar induced differential polyglot aphasia: a neurolinguistic and fMRI study. Brain Lang. 175, 18–28. https://doi.org/10.1016/j.bandl.2017.09.001.

Martino, A.D., Scheres, A., Margulies, D.S., Kelly, A.M.C., Uddin, L.Q., Shehzad, Z., Biswal, B., Walters, J.R., 2008. Functional Connectivity of Human Striatum : A Resting State fMRI Study. https://doi.org/10.1093/cercor/bhn041.

Molloy, E.K., Meyerand, M.E., Birn, R.M., 2014. The influence of spatial resolution and smoothing on the detectability of resting-state and task fMRI. Neuroimage 86, 221–230. https://doi.org/10.1016/j.neuroimage.2013.09.001.

Murphy, K., Fox, M.D., 2017. Towards a consensus regarding global signal regression for resting state functional connectivity MRI. Neuroimage 154, 169–173. https://doi.org/10.1016/j.neuroimage.2016.11.052.

Naeser, M.A., Martin, P.I., Theoret, H., Kobayashi, M., Fregni, F., Nicholas, M., Tormos, J.M., Steven, M.S., Baker, E.H., Pascual-Leone, A., 2011. TMS suppression of right pars triangularis, but not pars opercularis, improves naming in aphasia. Brain Lang. 119, 206–213. https://doi.org/10.1016/j.bandl.2011.07.005.

Noll, K.R., Sullaway, C., Ziu, M., Weinberg, J.S., Wefel, J.S., 2015. Relationships between tumor grade and neurocognitive functioning in patients with glioma of the left temporal lobe prior to surgical resection. Neuro Oncol. 17, 580–587. https://doi.org/10.1093/neuonc/nou233.

Otten, M.L., Mikell, C.B., Youngerman, B.E., Liston, C., Sisti, M.B., Bruce, J.N., Small, S.A., McKhann, G.M., 2012. Motor deficits correlate with resting state motor network connectivity in patients with brain tumours. Brain 135, 1017–1026. https://doi.org/10.1093/brain/aws041.

Paternostro-Sluga, T., Grim-Stieger, M., Posch, M., Schuhfried, O., Vacariu, G., Mittermaier, C., Bittner, C., Fialka-Moser, V., 2008. Reliability and validity of the Medical Research Council (MRC) scale and a modified scale for testing muscle strength in patients with radial palsy. J. Rehabil. Med. 40, 665–671. https://doi.org/10.2340/16501977-0235.

Pereira, F., Mitchell, T., Botvinick, M., 2009. Machine learning classifiers and fMRI: a tutorial overview. Neuroimage 45, S199–S209. https://doi.org/10.1016/j.neuroimage.2008.11.007.

Picart, T., Herbet, G., Moritz-Gasser, S., Duffau, H., 2018. Iterative surgical resections of diffuse glioma with awake mapping: how to deal with cortical plasticity and connectomal constraints? Neurosurgery. https://doi.org/10.1093/neuros/nyy218.

Power, J.D., Barnes, K.A., Snyder, A.Z., Schlaggar, B.L., Petersen, S.E., 2012a. Spurious but systematic correlations in functional connectivity MRI networks arise from subject motion. Neuroimage 59, 2142–2154. https://doi.org/10.1016/j.neuroimage.2011.10.018.

Power, J.D., Barnes, K.A., Snyder, A.Z., Schlaggar, B.L., Petersen, S.E., 2012b. NeuroImage Spurious but systematic correlations in functional connectivity MRI networks arise from subject motion. Neuroimage 59, 2142–2154. https://doi.org/10.1016/j.neuroimage.2011.10.018.

Power, J.D., Mitra, A., Laumann, T.O., Snyder, A.Z., Schlaggar, B.L., Petersen, S.E., 2014. Methods to detect, characterize, and remove motion artifact in resting state fMRI. Neuroimage 84, 320–341. https://doi.org/10.1016/j.neuroimage.2013.08.048.

Power, J.D., Schlaggar, B.L., Petersen, S.E., 2015. Recent progress and outstanding issues in motion correction in resting state fMRI. Neuroimage 105, 536–551. https://doi.org/10.1016/j.neuroimage.2014.10.044.

Ramsey, L.E., Siegel, J.S., Lang, C.E., Strube, M., Shulman, G.L., Corbetta, M., 2017. Behavioural clusters and predictors of performance during recovery from stroke. Nat. Hum. Behav. 1. https://doi.org/10.1038/s41562-016-0038.

Robles, S.G., Gatignol, P., Lehericy, S., Duffau, H., 2008. Long-term brain plasticity allowing a multistage surgical approach to World Health Organization Grade II gliomas in eloquent areas. J. Neurosurg. 109, 615–624. https://doi.org/10.3171/JNS/2008/109/10/0615.

Sanai, N., Mirzadeh, Z., Berger, M.S., 2008. Functional outcome after language mapping for glioma resection. N. Engl. J. Med. 358, 18–27. https://doi.org/10.1056/NEJMoa067819.

Sarubbo, S., Le Bars, E., Moritz-Gasser, S., Duffau, H., 2012. Complete recovery after surgical resection of left Wernicke's area in awake patient: a brain stimulation and functional MRI study. Neurosurg. Rev. 35, 287–292. discussion 292. https://doi.org/10.1007/s10143-011-0351-4.

Satterthwaite, T.D., Elliott, M.A., Gerraty, R.T., Ruparel, K., Loughead, J., Calkins, M.E., Eickhoff, S.B., Hakonarson, H., Gur, R.C., Gur, R.E., Wolf, D.H., 2013. NeuroImage an improved framework for confound regression and fi ltering for control of motion artifact in the preprocessing of resting-state functional connectivity data. Neuroimage 64, 240–256. https://doi.org/10.1016/j.neuroimage.2012.08.052.

Saur, D., Kreher, B.W., Schnell, S., Kummerer, D., Kellmeyer, P., Vry, M.S., Umarova, R., Musso, M., Glauche, V., Abel, S., Huber, W., Rijntjes, M., Hennig, J., Weiller, C., 2008. Ventral and dorsal pathways for language. Proc. Natl. Acad. Sci. USA 105, 18035–18040. https://doi.org/10.1073/pnas.0805234105.

Shen, X., Tokoglu, F., Papademetris, X., Constable, R.T., 2013. Groupwise whole-brain parcellation from resting-state fMRI data for network node identification. Neuroimage 82, 403–415. https://doi.org/10.1016/j.neuroimage.2013.05.081.

Siegel, J.S., Ramsey, L.E., Snyder, A.Z., Metcalf, N.V, Chacko, R.V, Weinberger, K., Baldassarre, A., Hacker, C.D., Shulman, G.L., Corbetta, M., 2016. Disruptions of network connectivity predict impairment in multiple behavioral domains after stroke. Proc. Natl. Acad. Sci. USA 113, E4367–E4376. https://doi.org/10.1073/pnas.1521083113.

Stam, C.J., 2014. Modern network science of neurological disorders. Nat. Rev. Neurosci. 15, 683–695. https://doi.org/10.1038/nrn3801.

Tan, L.H., Laird, A.R., Li, K., Fox, P.T., 2005. Neuroanatomical correlates of phonological processing of Chinese characters and alphabetic words: a meta-analysis. Hum. Brain Mapp. 25, 83–91. https://doi.org/10.1002/hbm.20134.

Taphoorn, M.J., Klein, M., 2004. Cognitive deficits in adult patients with brain tumours. Lancet Neurol. 3, 159–168. https://doi.org/10.1016/S1474-4422(04)00680-5.

Thiel, A., Habedank, B., Winhuisen, L., Herholz, K., Kessler, J., Haupt, W.F., Heiss, W.D., 2005. Essential language function of the right hemisphere in brain tumor patients. Ann. Neurol. 57, 128–131. https://doi.org/10.1002/ana.20342.

Tipping, M.E., 2000. The relevance vector machine. Advances in Neural Information Processing Systems. pp. 652–658.

Torres-Prioris, M.J., López-Barroso, D., Roé-Vellvé, N., Paredes-Pacheco, J., Dávila, G., Berthier, M.L., 2019. Repetitive verbal behaviors are not always harmful signs: compensatory plasticity within the language network in aphasia. Brain Lang. 190, 16–30. https://doi.org/10.1016/j.bandl.2018.12.004.

Tremblay, P., Dick, A.S., 2016. Broca and Wernicke are dead, or moving past the classic model of language neurobiology. Brain Lang. 162, 60–71. https://doi.org/10.1016/j.bandl.2016.08.004.

Triantafyllou, C., Hoge, R.D., Krueger, G., Wiggins, C.J., Potthast, A., Wiggins, G.C., Wald, L.L., 2005. Comparison of physiological noise at 1.5 T, 3 T and 7 T and optimization of fMRI acquisition parameters. Neuroimage 26, 243–250. https://doi.org/10.1016/j.neuroimage.2005.01.007.

Turkeltaub, P.E., Coslett, H.B., Thomas, A.L., Faseyitan, O., Benson, J., Norise, C., Hamilton, R.H., 2012. The right hemisphere is not unitary in its role in aphasia recovery. Cortex 48, 1179–1186. https://doi.org/10.1016/j.cortex.2011.06.010.

van Dellen, E., Douw, L., Hillebrand, A., Ris-Hilgersom, I.H.M., Schoonheim, M.M., Baayen, J.C., Hamer, P.C.D.W., Velis, D.N., Klein, M., Heimans, J.J., 2012. MEG network differences between low-and high-grade glioma related to epilepsy and cognition. PLoS One 7, e50122.

van Kessel, E., Baumfalk, A.E., van Zandvoort, M.J.E., Robe, P.A., Snijders, T.J., 2017. Tumor-related neurocognitive dysfunction in patients with diffuse glioma: a systematic review of neurocognitive functioning prior to anti-tumor treatment. J. Neurooncol. 134, 9–18. https://doi.org/10.1007/s11060-017-2503-z.

Vigneau, M., Beaucousin, V., Herve, P.Y., Duffau, H., Crivello, F., Houde, O., Mazoyer, B., Tzourio-Mazoyer, N., 2006. Meta-analyzing left hemisphere language areas: phonology, semantics, and sentence processing. Neuroimage 30, 1414–1432. https://doi.org/10.1016/j.neuroimage.2005.11.002.

Wang, J., Zuo, X., He, Y., 2010. Graph-based network analysis of resting-state functional MRI. Front. Syst. Neurosci. 4, 16. https://doi.org/10.3389/fnsys.2010.00016.

Warren, D.E., Power, J.D., Bruss, J., Denburg, N.L., Waldron, E.J., Sun, H., Petersen, S.E., Tranel, D., 2014. Network measures predict neuropsychological outcome after brain injury. Proc. Natl. Acad. Sci. 111, 14247–14252. https://doi.org/10.1073/pnas.1322173111.

Wen, P.Y., Macdonald, D.R., Reardon, D.A., Cloughesy, T.F., Sorensen, A.G., Galanis, E., Degroot, J., Wick, W., Gilbert, M.R., Lassman, A.B., Tsien, C., Mikkelsen, T., Wong, E.T., Chamberlain, M.C., Stupp, R., Lamborn, K.R., Vogelbaum, M.A., van den Bent, M.J., Chang, S.M., 2010. Updated response assessment criteria for high-grade gliomas: response assessment in neuro-oncology working group. J. Clin. Oncol. 28, 1963–1972. https://doi.org/10.1200/JCO.2009.26.3541.

Weng, H.H., Noll, K.R., Johnson, J.M., Prabhu, S.S., Tsai, Y.H., Chang, S.W., Huang, Y.C., Lee, J.D., Yang, J.T., Yang, C.T., Tsai, Y.H., Yang, C.Y., Hazle, J.D., Schomer, D.F., Liu, H.L., 2018. Accuracy of presurgical functional MR imaging for language mapping of brain tumors: a systematic review and meta-analysis. Radiology 286, 512–523. https://doi.org/10.1148/radiol.2017162971.

Winhuisen, L., Thiel, A., Schumacher, B., Kessler, J., Rudolf, J., Haupt, W.F., Heiss, W.D., 2007. The right inferior frontal gyrus and poststroke aphasia: a follow-up investigation. Stroke 38, 1286–1292. https://doi.org/10.1161/01.STR.0000259632.

04324.6c.
Wu, J., Lu, J., Zhang, H., Zhang, J., Yao, C., Zhuang, D., Qiu, T., Guo, Q., Hu, X., Mao, Y., Zhou, L., 2015. Direct evidence from intraoperative electrocortical stimulation indicates shared and distinct speech production center between Chinese and English languages. Hum. Brain Mapp. 36, 4972–4985. https://doi.org/10.1002/hbm.22991.
Xing, S., Lacey, E.H., Skipper-Kallal, L.M., Jiang, X., Harris-Love, M.L., Zeng, J., Turkeltaub, P.E., 2016. Right hemisphere grey matter structure and language outcomes in chronic left hemisphere stroke. Brain 139, 227–241. https://doi.org/10.1093/brain/awv323.
Xu, Y., Lin, Q., Han, Z., He, Y., Bi, Y., 2016. Intrinsic functional network architecture of human semantic processing: modules and hubs. Neuroimage 132, 542–555. https://doi.org/10.1016/j.neuroimage.2016.03.004.
Yan, C.G., Cheung, B., Kelly, C., Colcombe, S., Craddock, R.C., Di Martino, A., Li, Q., Zuo, X.N., Castellanos, F.X., Milham, M.P., 2013. A comprehensive assessment of regional variation in the impact of head micromovements on functional connectomics. Neuroimage 76, 183–201. https://doi.org/10.1016/j.neuroimage.2013.03.004.
Yan, C.G., Wang, X.D., Zuo, X.N., Zang, Y.F., 2016. DPABI: data processing & analysis for (resting-state) brain imaging. Neuroinformatics 14, 339–351. https://doi.org/10.1007/s12021-016-9299-4.
Yourganov, G., Fridriksson, J., Rorden, C., Gleichgerrcht, E., Bonilha, L., 2016. Multivariate connectome-based symptom mapping in post-stroke patients: networks supporting language and speech. J. Neurosci. 36, 6668–6679. https://doi.org/10.1523/JNEUROSCI.4396-15.2016.
Zhang, H., Shi, Y., Yao, C., Tang, W., Yao, D., Zhang, C., Wang, M., Wu, J., Song, Z., 2016. Alteration of the intra- and cross- hemisphere posterior default mode network in frontal lobe glioma patients. Sci. Rep. 6, 26972. https://doi.org/10.1038/srep26972.
Zhang, N., Xia, M., Qiu, T., Wang, X., Lin, C.P., Guo, Q., Lu, J., Wu, Q., Zhuang, D., Yu, Z., Gong, F., Farrukh Hameed, N.U., He, Y., Wu, J., Zhou, L., 2018. Reorganization of cerebro-cerebellar circuit in patients with left hemispheric gliomas involving language network: a combined structural and resting-state functional MRI study. Hum. Brain Mapp. 39, 4802–4819. https://doi.org/10.1002/hbm.24324.